Blood Flow Simulation in Patient-Specific Segmented Hepatic Arterial Tree

Costanza Simoncini, Yan Rolland, Valery Morgenthaler, Krzysztof Jurczuk, Hervé Saint-Jalmes, Pierre-Antoine Eliat, Marek Kretowski, Johanne Bezy-Wendling

Blood flow simulation in patient-specific segmented hepatic arterial tree

Costanza Simoncini[a,b,*], Yan Rolland[a,b,c], Valery Morgenthaler[d], Krzysztof Jurczuk[e], Hervé Saint-Jalmes[a,b], Pierre-Antoine Eliat[f,g,h], Marek Kretowski[e], Johanne Bezy-Wendling[a,b]

[a] *INSERM, U1099, Rennes, France*
[b] *Université de Rennes 1, LTSI, Rennes, France*
[c] *Centre Eugene Marquis, Rennes, France*
[d] *ANSYS, France*
[e] *Faculty of Computer Science, Bialystok University of Technology, Poland*
[f] *Université de Rennes 1, PRISM, Rennes, France*
[g] *Biosit, CNRS, UMS 3480, Rennes, France*
[h] *INSERM, UMS 018, Rennes, France*

Abstract

Purpose. Selective Internal Radiation Therapy is an emerging, minimally invasive therapy of liver cancer. Millions of microspheres are injected through a catheter into tumor vascular supply. Microspheres distribution in liver is strongly dependent on patient's arteries geometry and catheter tip positioning, which is currently chosen by the physician based on qualitative image interpretation. A patient-specific numerical simulation of blood flow would have a crucial importance in therapy optimization, allowing *in-silico* research of microspheres trajectories. *Material and methods.* We developed a procedure to segment patient's hepatic arterial vasculature with a Hessian based approach on 3D angiography, and to perform blood flow numerical simulation in the extracted geometry with ANSYS Fluent. In vivo blood velocity measurements were performed using phase contrast MRI to constrain these simulations. *Results.* Flow results in the larger vessels are coherent with literature, but very little is known for smaller arteries: simulation results are compared to velocity measures on hepatic arteries down to 2.2 mm of diameter on phase contrast MRI, which gave encouraging results for validation. *Conclusion.* A viable procedure for arteries segmentation and patient-specific blood flow simulation is proposed, phase contrast MRI allowing for tuning and validation of velocity values. The proposed personalized blood flow simulation is compulsory for the simulation of microspheres trajectories in the aim of tumor targeting.

Keywords: Computational fluid dynamics, hepatic artery, image processing, liver tumor, phase contrast MRI, radioembolization

*Corresponding author
Email address: costanza.simoncini@univ-rennes1.fr (Costanza Simoncini)

1. Introduction

Hepato-cellular carcinoma (HCC) is the fourth cause of mortality in the world. Treatment options are limited, less than 15% of patients are candidates for surgery and half of them for chemotherapy or radiotherapy [1]. A viable option to avoid side effects is the development of local treatments such as Selective Internal Radiation Therapy (SIRT) [13], which brings millions of radioactive microspheres directly into arterial tumor blood supply through a catheter, inducing far less embolizing syndrome than its equivalent in chemotherapy, and comparable (even better in an end-stage HCC) benefits [1]. The hepatic vascular supply is double: 25% comes from the hepatic artery and 75% from the portal vein. HCC is mainly vascularized by the hepatic artery. When the vessels irrigating the tumor are embolized, the arterial vascular supply of healthy liver can be also strongly reduced if the tumor targeting is not optimized. Therefore, if the portal supply does not compensate enough, post-embolisation syndrome can be severe.

Administration of SIRT requires a very precise knowledge of the hepatic arterial tree: currently, there is no available tool providing physicians the position where the catheter should be placed in the arterial tree, for the optimization of tumor targeting. In order to identify the best injection point, the physician realizes a cone-beam CT angiography to visualize the arteries geometry. When a therapy delivery point is chosen, biodegradable mock-spheres (Technetium ^{99m}Tc albumin macro-aggregated, MAA) are injected and a scintigraphy acquired one hour later reveals their distribution. The distribution of radioactive microspheres is thus approximately predicted from only one preliminary injection of ^{99m}Tc MAA, and for a same injection site, their behavior can actually be sometimes different [12]. Then, the simulation of several microspheres injection scenarii is of great interest for the clinician.

In the current work we aim at modeling arterial blood flow in a patient-specific hepatic arterial tree. This is a necessary step towards the patient-specific simulation of the distribution of the injected microspheres transported by blood. If the arteries segmentation is fine enough to detect the principal vessels irrigating the tumor, and if the simulation is initialized with patient-specific values of pressure or velocity, then the concentration of microspheres in the tumor can be more accurately estimated by existing appropriate CFD (computational fluid dynamics) methods.

It has been shown [4] that the distribution of microspheres at a bifurcation is not simply proportional to the blood flow distribution in the two descendant vessels, and that it can significantly

depend on the vessels geometry, which impacts on the flow streamlines and consequently on the particles trajectories. Blood flow characteristics like pressure and velocity can be deduced from angiography and through CFD if and only if we provide appropriate BC (boundary conditions) like pressure and/or velocity at the inlet and outlets of the vascular tree. This is why, to simulate the flow, we plan to combine these anatomic information with hemodynamics information extracted from PC MRI.

Of course, the vasculature and perfusion in tumors and healthy tissue is a key point to estimate the final microspheres (and thus dose) distributions. Nevertheless, the first step is to have the best estimation of velocity and pressure in the vessels upstream from such vasculature. Clearly the fluid and microspheres propagation in small vessels is far more complex to analyze, and for this reason we cannot expect to have access to a precise vessels network shape: based on angiographic data we can only expect, at this level, to segment the tumor regions, and this is not in the scope of this paper. Let us only indicate here that coupling real data and simulated data based on image characteristics could help solving this scale limitation, that could be achieved using a computational model of the finer vascular network, like the one we previously developed [19, 16].

A complete model of SIRT will let the radiologist simulate and quantify the distribution of microspheres in tumor and in healthy tissue, starting from any potential injection points and with different injection modalities, including dose amount and injection site and velocity.

Vessels enhancement from 3D angiography will be described in Section 2.1. Next, the creation of a triangular mesh for numerical simulation on the extracted geometry and the simulation setup are described in Section 2.2. Section 3 presents the principal results we obtained concerning blood flow and the preliminary validations we performed. As shown in Section 4, the procedure we developed opens the way to a patient-specific simulation of microspheres transport by blood flow, able to predict their distribution in liver depending on injection modalities and hemodynamic characteristics.

2. Method

Vessels extraction is performed on cone-beam CT 3D angiography. Data sets are up to $512 \times 512 \times 374$ voxels, and voxel size is $0.463 \times 0.463 \times 0.463$ mm. Images are acquired a few dozens of seconds after the injection of iodine-based contrast media, during the so-called arterial phase, i.e. when contrast agent is only in the arteries and is still not spread in all hepatic parenchyma. This acquisition gives a detailed portrait of the arterial tree until vessels with a diameter of around

0.5 mm.

All procedures involving human participants were in accordance with the ethical standards of the institutional research committee and with the 1964 Declaration of Helsinki. Approval by the institutional Medical Ethics Review Board and proper informed consent were obtained.

2.1. Patient-specific vasculature extraction

Arteries segmentation is performed by a first automatic enhancement of vessel structures using a 3D multiscale Frangi's algorithm [10]. Methods based on the analysis of the Hessian matrix are indeed shown to provide good segmentations results in most vascular cases, and the multiscale character of Frangi's filter is particularly suitable for hepatic vasculature, whose range of diameters is relatively large [15]. The algorithm is based on the idea that a given voxel belongs to a vessel if the local second derivative of the contrast function is low in a direction (i.e. along the direction of the vessel) and high in the two orthogonal directions (i.e. towards the walls of the vessel). This property can be exploited through an analysis of the eigenvalues (λ_1, λ_2, and λ_3) of an estimation of the Hessian matrix. In every voxel such matrix is obtained from second order finite differences, computed on the grey level image previously smoothed with a 3D Gaussian kernel. The size of this kernel is a scale parameter: a larger scale parameter corresponds to a more efficient smoothing. In particular, three geometrical characteristics are calculated from the eigenvalues in order to determine the tubular-like character of a given structure. $\mathcal{R}_\mathcal{A} = \frac{|\lambda_2|}{|\lambda_3|}$ indicates if it is closer to a plate-like or a line structure. $\mathcal{R}_\mathcal{B} = \frac{|\lambda_1|}{\sqrt{|\lambda_2\lambda_3|}}$ reflects its divergence from a blob-like form, and $\mathcal{S} = \sqrt{\sum_{j=1}^{3}\lambda_j^2}$ is used to distinguish vessels information from background noisy structures (the background noise becomes, after smoothing, a low and approximately constant grey level image, leading to small second order differences values). Frangi's filter computes the product of 3 monotonic nonlinear functions of, respectively $\mathcal{R}_\mathcal{A}$, $\mathcal{R}_\mathcal{B}$, and $\mathcal{S}$. The sensitivities of the filter to $\mathcal{R}_\mathcal{A}$, $\mathcal{R}_\mathcal{B}$, and $\mathcal{S}$ are tuned separately by three parameters. The efficient size of the smoothing parameter, i.e. of the scale parameter, depends on the vessel diameter. Therefore two other parameters have to be defined in this method, in order to take into account the size variability of the vessels: a scale range (depending on the diameters of the smallest and the largest vessel visible in the acquisition), and the scale ratio giving the step used to go through this range. We identified a set of parameters convenient for cone-beam CT angiography, given in Table 1. Vessels segmentation is then accomplished by a thresholding of the Frangi's enhanced image, followed by a partitioning of the resulting image into connected regions with a union-find algorithm (function

Table 1: Frangi's filter parameters for vessels enhancement

Scale range	Scale ratio	α	β	c
[1, 5]	0.5	0.5	0.9	500

"bwlabeln" in Matlab, where voxels are considered to belong to the same connected components if they are linked by at list one of their 26 neighbors). In order to reduce image noise, the classification into connected components requires a very low threshold, whose value is currently manually chosen based on the enhanced image histogram. The output of the this step corresponds to a 3D image where every connected component is labeled by a different grey level. The connected component corresponding to the arterial tree is then visually identified and extracted. This allows us to delete every enhanced structure that does not belong to the hepatic artery.

2.2. Blood flow simulation

We achieved patient-specific blood flow simulation in ANSYS Fluent (ANSYS, Inc., Canonsburg, PA). The conversion from an irregular segmented binary volume to a more regular meshed geometry, from which stable CFD simulations can be performed, is not straightforward and will be described below. Next, blood flow simulation setup will be outlined.

2.2.1. Mesh generation

In order to implement blood flow simulation with a CFD software, a closed smooth mesh is needed, where every surface corresponding to an input or output of blood flow must be separately defined. The binary volume resulting from the Frangi-based segmentation is thus used to create a triangular mesh corresponding to the surface of the segmented vessels. Input and outputs surfaces selection is achieved by a manual cut of the mesh at every vessel extremity. The result is a mesh describing a surface which is open at the entrance of blood and at every vessel end. A number of surfaces, called cap, corresponding to the number of mesh holes, needs to be created in order to perfectly close the open mesh. Such caps can be created thanks to the properties of the mesh: indeed, mesh consists of only triangles. When the mesh is clipped by a plane, new mesh nodes are created on the intersection between the mesh triangles and the plane, transforming some of the triangles into quadrilaterals. We developed an algorithm that first looks for all the mesh nodes which belong to a triangle or a quadrilateral, and which belong to only three facets or less. Such property guarantees that they are on the cut border of the mesh. All the identified border points

then need to be distinguished between every cap. A k-means clustering algorithm [3] accomplishes this step minimizing the average squared Euclidean distance into every group. Cap surfaces are created by a simple preliminary triangularization: for every set of nodes the barycenter is calculated, points are then classified in a trigonometric order, and triangles are finally defined by linking every point to its following neighbor and to the barycenter. Finally, quadrilaterals resulting from mesh clipping are split in two triangles in order to redefine a proper triangular mesh.

Afterwards, the surface corresponding to vessels wall and those corresponding to caps are imported in ANSYS Fluent meshing. A remeshing is performed using wrapping in order to obtain a smooth closed surface and mesh quality compatible with fluid simulations. Triangles minimum and maximum sizes can be adapted to the segmented vessels in order to smooth the surface or to better describe bifurcations and narrow vessels by choosing, respectively, a larger or smaller triangle size.

Different parameters for minimum and maximum sizes of the mesh elements were tested. A minimum size of 0.3 mm and a maximum one of 2.5 mm were chosen and give a good, smooth, representation of the geometry. In order to capture the behavior of the boundary layer with sufficient precision and reduce numerical instabilities, multiple layers of prisms are capping the artery walls. A volume mesh is generated on the basis of the surface mesh and passed to the ANSYS Fluent Solver, based on the finite volumes method.

2.2.2. Simulation setup

Blood is preliminarily considered as an incompressible Newtonian fluid. Its simulated viscosity value is defined as 0.004 Pa s, and its density as 1060 Kg /m^3 [20]. Inlet condition at the proper hepatic artery is given at mean arterial blood velocity, which is defined to be 30 cm/s over the entire vessel section. Different values are available in the literature [8, 23, 14, 18]. In such studies blood flow is measured in either the common, left or right hepatic artery, and the average velocity varies between 11 and 50 cm/s.

Due to the lack of an agreement in the literature concerning blood velocity values in hepatic vasculature, we measured it in the proper hepatic artery using a phase contrast (PC) MR sequence realized on a 1.5 T MR system (Aera, Siemens healthcare, Erlangen, Germany). Due to the retrospective nature of this study, it was not possible to acquire PC MRI on the same patients whose angiographies were analyzed, but the sequence was performed on a healthy volunteer in order to acquire in vivo velocity values. Phase contrast MRI has been used and improved since the eighties for blood flow measurements [6, 8, 5]. It is a gradient-echo sequence presenting bipolar gradients

aiming to encode blood velocity in any given direction. Thus, image contrast is proportional to blood velocity in the chosen spatial direction. In this study a 3D PC sequence was used, providing a time-averaged velocity in the three spatial directions without requiring too long acquisition times, prohibitive due to clinical constraints. The parameters of the sequence we acquired are given in Table 2. Velocity encoding value, corresponding to the maximum velocity that is to be acquired, was chosen as 80 cm/s in order to cover all the possible spectrum of mean physiological velocities in abdomen. The acquisition was performed on the axial plane and velocity in each of the three directions was encoded. The acquisition on the volunteer shows a velocity of 15 cm/s, which is

Table 2: Parameters of the 3D PC MRI sequence acquired for blood quantification in the hepatic artery

Acquisition type	3D
Slice thickness	1.3 mm
Pixel size	1.6 mm $\times$ 1.6 mm
Repetition time	51.75 ms
Echo time	4.56 ms
Flip angle	15
Acquisition plane	axial
Velocity encoding	80 cm/s

coherent with measurements in [8]. Output boundary conditions are given on blood flow percentage, as to be proportional to every outlet vessel diameter. Classical no-slip conditions are enforced on vessel walls.

Navier-Stokes Equations are finally solved in ANSYS Fluent. Due to the relatively low velocities, a pressure-based solver was used together with a segregated SIMPLE (Semi-Implicit Method for Pressure-Linked Equations) scheme [17]. The convergence is verified by checking the mass and momentum conservation in between inlet and outlets. Calculation are stopped when a difference of 10^{-7} for continuity and 10^{-4} for momentum is reached. To enhance convergence, a Least-Square Gradient Method was chosen. Such method is comparable to the one of the node-based gradient on skewed and distorted unstructured meshes and is less expensive to compute [21].

3. Results

The procedure was applied to the cone-beam angiographies of 4 patients suffering from an advanced stage HCC, as can be seen in Figures 1 and 2.

3.1. Extraction of patient's data

Cone-beam angiographies of 2 of the 4 patients are shown in Fig. 1a and Fig. 2a through a Volume Rendering technique. Patient's tumor and the vessels that irrigate it are clearly visible. It can be noticed in Fig. 1 that the vessels supplying blood to the tumor are more numerous and more irregular, due to tumor angiogenesis. Moreover, metallic clips near the patient's tumor make the image particularly noisy and complicate the segmentation of the tumor vessels.

Vessels segmentation results in arterial trees with 20 to 50 outlet vessels. Radius of the proper hepatic artery varies between 2.3 and 3.6 mm. The smallest radius of segmented vessels is 0.49 mm. Details about the obtained mesh are given in Table 3 for all the patients.

Table 3: Mesh characteristics for the hepatic arteries of the four patients

	Patient 1	Patient 2	Patient 3	Patient 4
Number of outlets	24	20	29	50
Number of faces	2133552	968791	1353653	3995926
Number of nodes	288175	130792	187330	540732
Min. face area (mm^2)	2.5 e^{-3}	1.1 e^{-3}	1.9 e^{-3}	1.1 e^{-3}
Max. face area (mm^2)	0.56	0.298	0.589	0.47

3.2. Flow simulation results

Blood flow simulation was performed on a portable computer equipped with the quad-core Intel Core i7-2820QM CPU (2.3 GHz) and 16 GB of RAM. Computational time of simulation varied between 15 and 45 minutes on 3 cores. Table 4 shows area-weighted average pressure and velocity values for all the 4 patients, as well as segmented vessels radii. Data are given, for each patient, for the blood inlet surface (proper hepatic artery) and for the outlets average. Fig. 1b and 2b illustrate the contours of absolute pressure in the geometries extracted from the angiographies of Patients 1

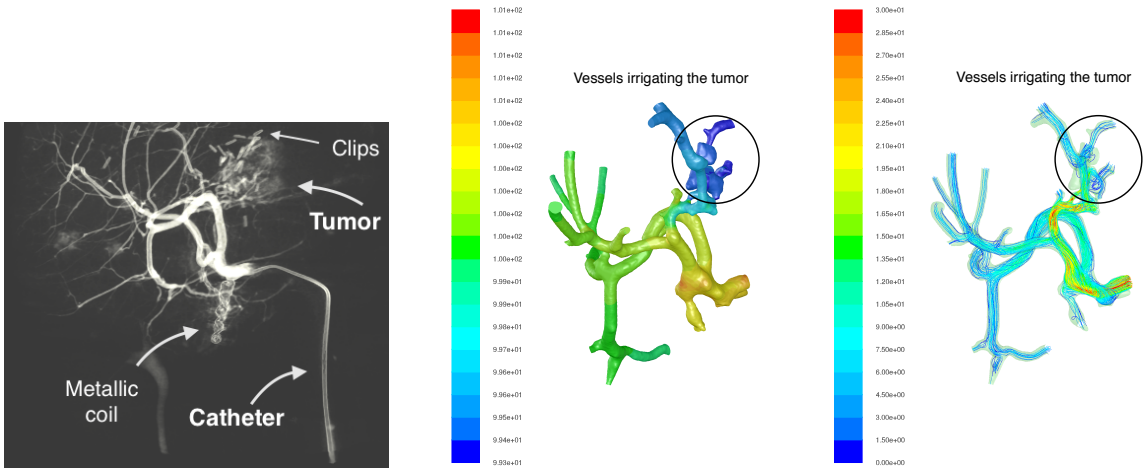

(a) Cone-beam CT 3D angiography (Centre Eugène Marquis, Rennes, France)

(b) Pressure field (mmHg)

(c) Pathlines colored by velocity magnitude (cm/s)

Figure 1: Cone-beam angiography and blood flow simulation results on segmented arterial tree for Patient 1

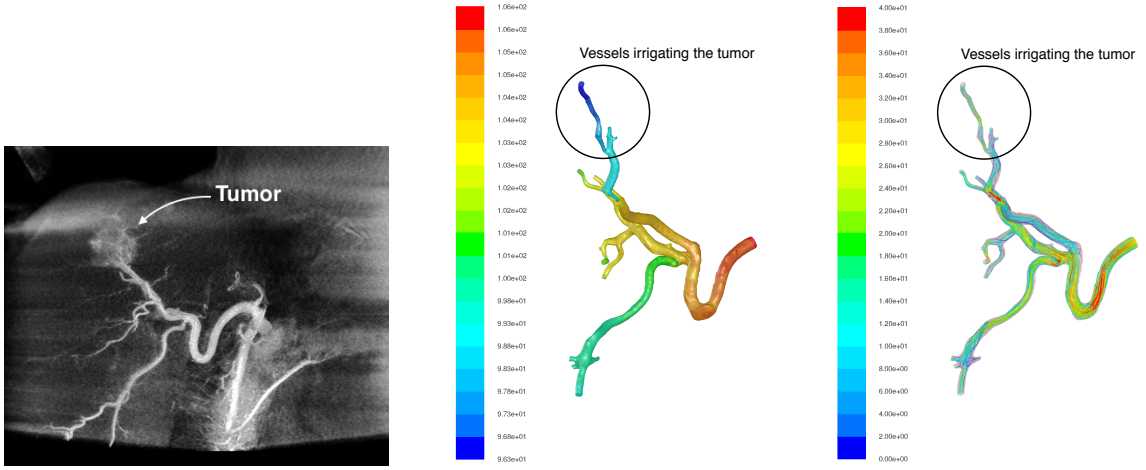

(a) Cone-beam CT 3D angiography (Centre Eugène Marquis, Rennes, France)

(b) Pressure field (mmHg)

(c) Pathlines colored by velocity magnitude (cm/s)

Figure 2: Cone-beam angiography and blood flow simulation results on segmented arterial tree for Patient 2

and 2. Velocity results for the same patients are shown in Fig. 1c and 2c, where blood pathlines are colored based on velocity magnitude.

3.3. Validation

Pressure and velocity values at the entrance of the proper hepatic artery are coherent with literature [9], whereas blood flow characteristics farther in the hepatic arterial tree (i.e. for smaller

Table 4: Radius, area-weighted average pressure and velocity results in segmented arterial trees of the 4 patients

		Patient 1	**Patient 2**	**Patient 3**	**Patient 4**
Radius (mm)	Inlet	2.6	2.3	3.6	3.6
	Min. of outlets	0.6	0.49	0.5	0.9
	Max. of outlets	2.7	1.3	2.4	2.2
	Average of outlets	1.7 ± 0.6	0.8 ± 0.2	1.2 ± 0.5	1.5 ± 0.3
Pressure (mmHg)	Inlet	100.4	106	103	102
	Min. of outlets	99.3	96.4	99	99. 3
	Max. of outlets	100.3	104.5	101.8	101.7
	Average of outlets	99.8 ± 0.3	101.4 ± 2.1	100 ± 0.7	100 ± 0.6
Velocity (cm/s)	Inlet	30	30	30	30
	Min. of outlets	2.7	11.7	6.9	3.2
	Max. of outlets	4.4	19.8	19.4	4.8
	Average of outlets	2.8 ± 0.3	12.7 ± 1.7	8.4 ± 2.3	3.3 ± 0.2

diameters) are poorly documented. Approximate information relying pressure and velocity to vessels diameter in human systemic circuit exists. Pressure of arteries at sizes as those analyzed in current study can vary approximately between 70 and 100 mmHg [7]. Information about blood velocity at small hepatic arteries is also hard to determine exactly. According to [7], mean blood velocity for arteries whose diameter varies between 2 and 6 mm, can vary between 20 and 50 cm/s. To address this hindrance, we performed preliminary MRI phase contrast acquisition on healthy volunteer which gave the results shown in Table 5 concerning mean blood velocity until a vessel diameter of 2.2 mm.

In order to justify the choice of the output boundary conditions of the simulations, the ratios between diameter and blood flow in vessels of similar sizes were also observed. It is well known that vessels of different sizes (aorta, arteries, arterioles,...) have different blood flow behaviors, this is why only vessels with similar sizes were compared. Even if the velocity measurements on PC MRI were possible only on vessels much larger that the outputs of the simulation, we verified that our choice of boundary conditions was reasonable. The ratios between diameter and blood flow are similar in all considered vessels, except in the left hepatic artery. Nevertheless, the diameter of this vessel is smaller and, consequently, the measurement less reliable.

Table 5: Blood flow velocity measured on phase contrast MRI acquisition on a 27 years old healthy volunteer

	Diameter	**Mean blood velocity**	**Ratio between diameter and flow ratio**
Abdominal aorta	1.5 cm	21 cm/s	-
Inferior vena cava	1.1 cm	19.4 cm/s	-
Celiac trunk	7 mm	35 cm/s	-
Common hepatic artery	3.1 mm	15.5 cm/s	44
Gastroduodenal artery	3 mm	12 cm/s	59
Right hepatic artery	2.8 mm	12.9 cm/s	59
Left hepatic artery	2.2 mm	9.8 cm/s	98
Splenic artery	3 mm	13.7 cm/s	51

4. Discussion and conclusion

We developed a procedure to extract a patient-specific hepatic arterial tree from cone-beam CT 3D angiography, until a vessel diameter of around 0.5 mm. We realized blood flow simulation, the results of which appear to be coherent with the literature, even if flow precise characteristics at such level are very little known and vary significantly between different individuals. Our MRI measurements are not statistically representative but are validated by an experienced radiologist and by known mean velocities at the aorta and inferior vena cava levels [11]. Their interest is double: information about blood velocity at smaller arteries is crucial for the definition of boundary conditions, by letting us tuning output conditions that are currently little known, in particular tumors blood flow. Output conditions would be adjusted in order to obey to some data fidelity relative to velocity measured on PC MRI. Moreover, it will let us validate blood flow results.

Different approaches, not considered in this paper, exist for the estimation of boundary conditions. For example, Aramburu et al. [2] introduce a perfusion simplified 2 parameters model in order to complete a 0-D model version of the flow in the imaged tree. The parameters identification requires the knowledge of synchronised values of pressure and flow rate at the inlet and at different phases of the cardiac cycle (systolic and diastolic phases).

We plan to undertake a clinical study on blood flow measurements, optimizing phase contrast MRI sequence. A better image resolution can be achieved by synchronizing the acquisition to breathing and by choosing a velocity encoding value tuned to the patient's peculiarities (obesity,

cirrhosis, HCC can have an influence on blood flow). Phase contrast sequence is not currently included in the clinical protocol for HCC, but such clinical study will allow us to apply the described procedure to patients who have undertaken both cone-beam CT angiography and MRI phase contrast, which was not possible for the current study due to its retrospective nature. Moreover, new 4D PC MRI techniques, not yet available on the MR system used for this study, should allow time-resolved acquisitions of three dimensional PC MRI, synchronized to the cardiac cycle [22]. It should be noticed though, that time constraints in the clinical workflow do not actually encourage this approach.

A more precise description of variable blood viscosity and pulsatility will also be performed. Moreover, before SIRT, patients can undertake chemoembolization, vessels coiling or clipping whose metal can induce artifacts in acquisitions and reduce the quality of the segmentation, as for Patient 1, where the diameters of tumor vessels near the clips are overestimated. Results are inevitably dependent on segmentation, which is currently validated by placing a mask on the original image, and whose tuning is still operator-dependent. In particular, the choice of the low threshold needed before the classification into connected components influences the final segmentation especially concerning smaller vessels, whose diameter may be overestimated. In the future an adaptive thresholding method like the Otsu's method or the Kuwahara filter will be used in order to extract more realistic vessels diameters and too complex tumor vessels may not be segmented but simulated by the vascular model [19, 16] instead.

Hepatic artery diameters are, for the four patients, larger than the average, which is assessed at 3.8 ± 0.8 in [23] for healthy patients. This can be explained by the presence of cirrhosis and HCC, which can induce a more important blood flow in liver arteries and, in turn, a larger diameter of the proper hepatic artery. The patient-specific blood flow simulations described in this paper represent a preliminary, compulsory step that will allow us to to perform, under the same boundary conditions and taking into account every patient's peculiarities, an accurate numerical simulation of SIRT microspheres transport in the patient's hepatic arterial tree, thanks to the Fluent particles transport tools. In particular, we envisage a computation of particles trajectories based on a Lagrangian particles tracking approach, that would take into account all the forces acting on the microspheres as fluid drag force and gravity. On the other side, the influence of microspheres on blood flow can be neglected due to the large ratio between the diameters of vessels and microspheres and the low microspheres density. Such simulations have a crucial importance for physicians in the aim of tumor targeting.

Acknowledgment

The authors would like to thank Jean-Jacques Bellanger, Jean-Claude Nunes and Michel Rochette for their precious help in this work.

Funding: This research did not receive any specific grant from funding agencies in the public, commercial, or not-for-profit sectors.

Disclosure: Each author has materially participated in the research and article preparation. All authors have approved the final article. The authors have no conflict of interest. V. Morgenthaler is employed by ANSYS.

References

[1] Andreana, L., Isgrò, G., Marelli, L., Davies, N., Yu, D., Navalkissoor, S., Burroughs, A. K., oct 2012. Treatment of hepatocellular carcinoma (HCC) by intra-arterial infusion of radio-emitter compounds: trans-arterial radio-embolisation of HCC. Cancer Treat. Rev. 38 (6), 641–9.

[2] Aramburu, J., Antón, R., Rivas, A., Ramos, J. C., Sangro, B., Bilbao, J. I., Anton, R., Rivas, A., Ramos, J. C., Sangro, B., Bilbao, J. I., 2016. Liver cancer arterial perfusion modelling and CFD boundary conditions methodology: a case study of the haemodynamics of a patient-specific hepatic artery in literature-based healthy and tumour-bearing liver scenarios. Int. j. numer. method. biomed. eng., 807–827.

[3] Arthur, D., Vassilvitskii, S., 2007. K-means++: The Advantages of Careful Seeding. SODA '07 Proc. eighteenth Annu. ACM-SIAM Symp. Discret. algorithms, 1027–1035.

[4] Basciano, C. A., Kleinstreuer, C., Kennedy, A. S., Dezarn, W. A., Childress, E., may 2010. Computer modeling of controlled microsphere release and targeting in a representative hepatic artery system. Ann. Biomed. Eng. 38 (5), 1862–79.

[5] Bollache, E., Kachenoura, N., Frouin, F., Redheuil, A., Mousseaux, E., Lucor, D., 2013. Numerical modeling of arterial pulse wave propagation to characterize aortic hemodynamic: Validation using magnetic resonance data. Irbm 34 (1), 86–89.
URL http://dx.doi.org/10.1016/j.irbm.2012.12.008

[6] Bryant, D., Payne, A., Firmin, D., Longmore, D., 1984. Measurement of flow with NMR imaging using a gradient pulse and phase difference technique. J. Comput. Assist. Tomogr.

8 (4), 588–593.
URL http://www.ncbi.nlm.nih.gov/pubmed/6736356

[7] Bura-Rivière, A., Boccalon, H., 2010. Physiologie et exploration de la circulation artérielle. Angeiologie 6 (1), 1–22.

[8] Dyvorne, H. A., Knight-Greenfield, A., Besa, C., Cooper, N., Garcia-Flores, J., Schiano, T. D., Taouli, B., 2015. Quantification of hepatic blood flow using a high-resolution phase-contrast MRI sequence with compressed sensing acceleration. AJR Am. J. Roentgenol. 204 (3), 510–518.
URL www.ncbi.nlm.nih.gov/pmc/articles/PMC4341958/

[9] Ficher, A., 1963. The Liver. Elsevier.

[10] Frangi, A. F., Niessen, W. J., Vincken, K. L., Viergever, M. A., 1998. Multiscale vessel enhancement filtering. Medial Image Comput. Comput. Assist. Invervention 1496, 130–137.

[11] Gabe, B. I. T., Gault, J. H., Ross, J., Mason, D. T., Mills, C. J., Sc, B., Schillingford, J. P., Braunwald, E., Al, G. E. T., 1969. Measurement of Instantaneous Blood Flow Velocity and Pressure in Conscious Man with a Catheter-Tip Velocity Probe. Circ. - J. Am. Hear. Assoc. XL (5), 603–614.

[12] Garin, E., Rolland, Y., Lenoir, L., Pracht, M., Mesbah, H., Porée, P., Laffont, S., Clement, B., Raoul, J.-L., Boucher, E., jan 2011. Utility of Quantitative Tc-MAA SPECT/CT for yttrium-Labelled Microsphere Treatment Planning: Calculating Vascularized Hepatic Volume and Dosimetric Approach. Int. J. Mol. Imaging 2011, 398051

[13] GroupHealth, 2014. Clinical Review Criteria. SIRT (Selective Internal Radiation Therapy) Therasphere and SIR Sphere for Unresectable Hepatocellular Carcinoma.

[14] Hubner, G. H., Steudel, N., Kleber, G., Behrmann, C., Lotterer, E., Fleig, W. E., 2000. Hepatic arterial blood flow velocities: assessment by transcutaneous and intravascular Doppler sonography. J. Hepatol. 32, 893–899.

[15] Jimenez-Carretero, D., Santos, A., Kerkstra, S., Rudyanto, R. D., Ledesma-Carbayo, M. J., 2013. 3D Frangi-based lung vessel enhancement filter penalizing airways. In: Biomed. Imaging (ISBI), 2013 IEEE 10th Int. Symp. pp. 926–929.

[16] Jurczuk, K., Kretowski, M., Eliat, P.-A., Saint-Jalmes, H., Bézy-Wendling, J., 2014. In Silico Modeling of Magnetic Resonance Flow Imaging in Complex Vascular Networks. Med. Imaging, IEEE Trans. 33 (11), 2191–2209.
URL http://www.ncbi.nlm.nih.gov/pubmed/25020068

[17] Karki, K. C., Patankar, S. V., 1989. Pressure based calculation procedure for viscous flows at all speedsin arbitrary configurations. AIAA J. 27 (9), 1167–1174.

[18] Kito, Y., Nagino, M., Nimura, Y., 2001. Doppler sonography of hepatic arterial blood flow velocity after percutaneous transhepatic portal vein embolization. AJR. Am. J. Roentgenol. 176 (4), 909–912.

[19] Kretowski, M., Rolland, Y., Bézy-Wendling, J., Coatrieux, J.-L., feb 2003. Physiologically based modeling of 3-D vascular networks and CT scan angiography. IEEE Trans. Med. Imaging 22 (2), 248–57.
URL www.ncbi.nlm.nih.gov/pubmed/12716001

[20] Levick, J. R., 2013. An Introduction to Cardiovascular Physiology. Elsevier Science.

[21] Rausch, R. D., Batina, J. T., Yang, H. T. Y., 1992. Spatial Adaptation of Unstructured Meshes for Unsteady Aerodynamic Flow Computations. AIAA J. 30 (5), 1243–1251.

[22] Stankovic, Z., Allen, B. D., Garcia, J., Jarvis, K. B., Markl, M., 2014. 4D flow imaging with MRI. Cardiovasc. Diagn. Ther. 4 (2), 173–92.
URL www.ncbi.nlm.nih.gov/pubmed/24834414

[23] Tziafalia, C., Vlychou, M., Tepetes, K., Kelekis, N., Fezoulidis, I. V., 2006. Echo-Doppler measurements of portal vein and hepatic artery in asymptomatic patients with hepatitis B virus and healthy adults. J. Gastrointestin. Liver Dis. 15 (4), 343–6.